

Magnitude and crystalline anisotropy of hole magnetization in (Ga,Mn)As

C. Śliwa*

*Institute of Physics, Polish Academy of Sciences,
al. Lotników 32/46, PL 02-668 Warszawa, Poland*

T. Dietl†

*Institute of Physics, Polish Academy of Sciences and ERATO Semiconductor Spintronics Project,
Japan Science and Technology, al. Lotników 32/46, PL 02-668 Warszawa, Poland and
Institute of Theoretical Physics, Warsaw University, PL 00-681 Warszawa, Poland*

(Dated: January 3, 2018)

Theory of hole magnetization M_c in zinc-blende diluted ferromagnetic semiconductors is developed relaxing the spherical approximation of earlier approaches. The theory is employed to determine M_c for (Ga,Mn)As over a wide range of hole concentrations and a number of crystallographic orientations of Mn magnetization. It is found that anisotropy of M_c is practically negligible but the obtained magnitude of M_c is significantly greater than that determined in the spherical approximation. Its sign and value compares favorably with the results of available magnetization measurements and ferromagnetic resonance studies.

I. INTRODUCTION

Following the discovery of ferromagnetism in zinc-blende Mn-based semiconducting compounds,¹ a theory has been developed that describes correctly a number of properties of those materials.^{2,3} The theory, which is based on the Zener model of ferromagnetism mediated by band carriers, takes into account the complex structure of the valence band of zinc-blende semiconductors *via* the $\mathbf{k} \cdot \mathbf{p}$ method, and employs the molecular-field and virtual-crystal approximations to include the exchange interaction between the Mn d electrons and the valence band holes.^{2,4} In particular, the magnetic moment of the hole carriers per unit volume, $M_c(p)$, has been calculated for a range of hole concentrations p .² The results,² corroborated recently by an independent calculation,⁵ have shown that while a part of this magnetic moment can be attributed to spin polarization of the hole Fermi liquid, the orbital magnetic moment of the holes has also to be taken into account. However, in order to reduce a differential multi-band Landau equation to an algebraic one, it has been assumed in Refs. 2 and 5 that two relevant Luttinger parameters have the same value, $\gamma_2 = \gamma_3$. A quantitative error introduced but this approximation has been hard to estimate and, moreover, within such an approximation a significant warping of the valence band has been neglected.

Motivated by the recent accurate magnetization measurements carried out by Sawicki and co-workers⁵ and ferromagnetic resonance studies of Liu *et al.*,⁶ both completed for high quality (Ga,Mn)As, we have decided to develop theory of hole magnetization in carrier-controlled ferromagnetic semiconductors valid for the arbitrary values of γ_2 and γ_3 . Our results show that in the experimentally relevant range of hole concentrations the theoretical values of $M_c(p)$ are much greater than those evaluated previously,^{2,5} which allows us for a better description of the experimental findings.^{5,6} Furthermore, we find that the crystalline anisotropy of $M_c(p)$ is practically negli-

gible, so that the dipole interaction between the subsystems of Mn and hole magnetic moments does not contribute to magnetic anisotropy of (Ga,Mn)As.

The calculation proceeds by the determination of the partition function of the holes occupying the Landau levels in the presence of Mn spontaneous magnetization \mathbf{M} , assumed to be parallel to the external magnetic field \mathbf{B} . Hole magnetization is then obtained by differentiating the Gibbs thermodynamic potential with respect to \mathbf{B} . In contrast to the case $\gamma_2 = \gamma_3$, a significant amount of symbolic calculations involving trigonometric expressions is required, followed by an efficient numerical solution of a truncated infinite eigenvalue problem. This methodology allows us to calculate and examine hole magnetization for various crystallographic directions of the magnetic field and magnetization of the Mn-sublattice.

The remaining part of this paper is organized as follows: in Section II we present the details of the valence band structure of a zinc-blende semiconductor; in Section III we discuss quantized motion of an electron in uniform magnetic field; in Section IV we describe some technicalities of our algorithm; in Section V we present our results, and finally in Section VI we present conclusions of our work.

II. THE $\mathbf{k} \cdot \mathbf{p}$ MODEL OF THE VALENCE BAND

Following classic works of Luttinger⁷ as well as of Bell and Rogers⁸ and Pidgeon and Brown,⁹ the energy states in semiconductors of zinc-blende structure in a magnetic field (specifically InSb) have been considered in detail by Trebin, Rössler, and Ranvaud,¹⁰ who obtained the effective mass Hamiltonian taking into account the two-fold degenerate conduction band of the symmetry Γ_6 , the four-fold degenerate uppermost valence band of the symmetry Γ_8 , and the two-fold degenerate split-off valence band of the Γ_7 symmetry. A model in which an upper

$$\begin{aligned}
T_x &= \frac{1}{3\sqrt{2}} \begin{pmatrix} -\sqrt{3} & 0 & 1 & 0 \\ 0 & -1 & 0 & \sqrt{3} \end{pmatrix} & T_y &= \frac{-i}{3\sqrt{2}} \begin{pmatrix} \sqrt{3} & 0 & 1 & 0 \\ 0 & 1 & 0 & \sqrt{3} \end{pmatrix} & T_z &= \frac{\sqrt{2}}{3} \begin{pmatrix} 0 & 1 & 0 & 0 \\ 0 & 0 & 1 & 0 \end{pmatrix} \\
T_{xx} &= \frac{1}{3\sqrt{2}} \begin{pmatrix} 0 & -1 & 0 & \sqrt{3} \\ -\sqrt{3} & 0 & 1 & 0 \end{pmatrix} & T_{yy} &= \frac{1}{3\sqrt{2}} \begin{pmatrix} 0 & -1 & 0 & -\sqrt{3} \\ \sqrt{3} & 0 & 1 & 0 \end{pmatrix} & T_{zz} &= \frac{\sqrt{2}}{3} \begin{pmatrix} 0 & 1 & 0 & 0 \\ 0 & 0 & -1 & 0 \end{pmatrix} \\
T_{yz} &= \frac{i}{2\sqrt{6}} \begin{pmatrix} -1 & 0 & -\sqrt{3} & 0 \\ 0 & \sqrt{3} & 0 & 1 \end{pmatrix} & T_{zx} &= \frac{1}{2\sqrt{6}} \begin{pmatrix} -1 & 0 & \sqrt{3} & 0 \\ 0 & \sqrt{3} & 0 & -1 \end{pmatrix} & T_{xy} &= \frac{i}{\sqrt{6}} \begin{pmatrix} 0 & 0 & 0 & -1 \\ -1 & 0 & 0 & 0 \end{pmatrix}
\end{aligned}$$

TABLE I: Matrices for the cross space of the valence and split-off valence band states ($U_i = T_i^\dagger$, $U_{ij} = T_{ij}^\dagger$).

Γ_8 and Γ_7 conduction bands are explicitly included was developed by Pfeffer and Zawadzki.¹¹

Here, we consider explicitly only the valence band, namely the bands of the Γ_8 and Γ_7 symmetry, denoted respectively as v and s , for which we choose the basis $(|\frac{3}{2}, \frac{3}{2}\rangle, |\frac{3}{2}, \frac{1}{2}\rangle, |\frac{3}{2}, -\frac{1}{2}\rangle, |\frac{3}{2}, -\frac{3}{2}\rangle, |\frac{1}{2}, \frac{1}{2}\rangle, |\frac{1}{2}, -\frac{1}{2}\rangle)$.¹⁴ Therefore, in our $\mathbf{k} \cdot \mathbf{p}$ model of the valence band of a zinc-blende semiconductor, the band electron Hamiltonian has the block form

$$\mathcal{H} = \begin{pmatrix} \mathcal{H}^{vv} & \mathcal{H}^{vs} \\ \mathcal{H}^{sv} & \mathcal{H}^{ss} \end{pmatrix}, \quad (1)$$

where

$$\begin{aligned}
\mathcal{H}^{vv} &= -\frac{\hbar^2}{m} \left\{ \frac{1}{2} \gamma_1 k^2 - \gamma_2 \left[(J_x^2 - \frac{1}{3} J^2) k_x^2 + c.p. \right] \right. \\
&\quad \left. - 2\gamma_3 \{ J_x, J_y \} \{ k_x, k_y \} + c.p. \right\} \\
&\quad - \frac{e\hbar}{m} \kappa (\mathbf{J} \cdot \mathbf{B}), \quad (2)
\end{aligned}$$

$$\begin{aligned}
\mathcal{H}^{ss} &= -(\Delta_0 + \frac{\hbar^2}{2m} \gamma_1 k^2) \\
&\quad - \frac{e\hbar}{m} (\kappa + \frac{g_0}{4}) (\boldsymbol{\sigma} \cdot \mathbf{B}), \quad (3)
\end{aligned}$$

$$\begin{aligned}
\mathcal{H}^{vs} &= \frac{\hbar^2}{m} \left[-3\gamma_2 (U_{xx} k_x^2 + c.p.) \right. \\
&\quad \left. - 6\gamma_3 (U_{xy} \{ k_x, k_y \} + c.p.) \right] \\
&\quad + \frac{3e\hbar}{2m} (\kappa + \frac{g_0}{2}) (\mathbf{U} \cdot \mathbf{B}). \quad (4)
\end{aligned}$$

Here, $\{A, B\} = \frac{1}{2}(AB + BA)$ and c.p. denotes cyclic permutations. The matrices J_i are the spin- $\frac{3}{2}$ angular momentum matrices, σ_i are the spin- $\frac{1}{2}$ angular momentum matrices multiplied by 2 (Pauli matrices in our basis), and T_i , T_{ij} are the cross space matrices introduced in Ref. 10, in our basis given in Table I (which corrects one misprinted sign in Ref. 10, Table I). Notice the Zeeman terms of the form given in Ref. 2 that properly accounts for the Landé factor of the free electron, g_0 , a correction in the overall sign of \mathcal{H}^{vs} , as well as the factor of two in the first (kinetic) term of \mathcal{H}^{vs} that has changed with respect to Ref. 10.

Now, to complete our model with the exchange interaction between the valence band carriers and the localized d -electron spins, treated within the molecular-field and virtual-crystal approximations, we augment our Hamiltonian with the p - d exchange matrix \mathcal{H}_{pd} ,

$$\mathcal{H}_{pd} = B_G \begin{pmatrix} 2(\mathbf{J} \cdot \mathbf{w}) & 6(\mathbf{U} \cdot \mathbf{w}) \\ 6(\mathbf{T} \cdot \mathbf{w}) & -(\boldsymbol{\sigma} \cdot \mathbf{w}) \end{pmatrix}, \quad (5)$$

where the B_G parameter is proportional to the Mn magnetization M and the p - d coupling constant β ,

$$B_G = A_F \frac{\beta M}{6g\mu_B}, \quad (6)$$

where $A_F \approx 1.2$ is the Fermi liquid Landau parameter describing effects of the hole-hole exchange interaction,^{2,3} and \mathbf{w} is the versor pointing in the direction of the Mn magnetization; see Ref. 2, Eqs. A13 to A18.

III. QUANTIZED MOTION OF AN ELECTRON IN UNIFORM MAGNETIC FIELD

The differential operators k_i in our $\mathbf{k} \cdot \mathbf{p}$ model are

$$k_\alpha = -i \frac{\partial}{\partial x_\alpha} + \frac{eA_\alpha}{\hbar}, \quad (7)$$

and satisfy $\mathbf{k} \times \mathbf{k} = e\mathbf{B}/i\hbar$, or

$$\varepsilon_{\alpha\beta\gamma} k_\beta k_\gamma = \frac{eB_\alpha}{i\hbar}. \quad (8)$$

Following Luttinger⁷, by

$$a = \frac{1}{\sqrt{2s}} (k_1 - ik_2), \quad (9)$$

$$a^\dagger = \frac{1}{\sqrt{2s}} (k_1 + ik_2), \quad (10)$$

we introduce a pair of operators (a, a^\dagger) satisfying the canonical commutation relation, $[a, a^\dagger] = 1$. Here, $s = eB/\hbar$, and the coordinate system “1”, “2”, “3” is such that \mathbf{B} is along the “3” direction. Then, $k_H = k_3$ (the momentum component along the direction of the magnetic field) commutes with a and a^\dagger . We will express the effective mass Hamiltonian in terms of (a, a^\dagger, k_H) .

In the Landau gauge, the eigenvalues of $n = a^\dagger a$, together with k_1 and k_3 , number the energy levels (Landau levels) for a free electron in the uniform magnetic field \mathbf{B} . The corresponding wavefunctions are given by¹²

$$\psi = \exp[i(k_1 x_1 + k_3 x_3)] u_n(x_2 - \bar{x}_2), \quad (11)$$

where $u_n(y) = (s/\pi)^{1/4} \exp(-sy^2/2) H_n(\sqrt{sy}) / \sqrt{2^n n!}$ is the wavefunction of a harmonic oscillator, and $\bar{x}_2 = k_1/s$. Since the vector potential $\mathbf{A}(\mathbf{x}) = (-Bx_2, 0, 0)$ does not depend on x_1 and x_3 , we use periodic boundary conditions for those two variables. As far as x_2 is concerned,

the particle is localized by the magnetic field, therefore the boundary conditions can be ignored (at least in the thermodynamic limit, *i.e.* when the magnetic length is much smaller than the size of the system). On the other hand, the length of the system in the “2” direction determines the range of integration over k_1 . Hence, we have the formula (B3) of Ref. 2:

$$G_c = -k_B T \frac{eB}{2\pi\hbar} \int_{-\infty}^{\infty} \frac{dk_H}{2\pi} \sum_{i=0}^{\infty} \log\{1 + \exp[\frac{\varepsilon_i(k_H) - \varepsilon_F}{k_B T}]\}, \quad (12)$$

where we have changed the sign under exponent to reflect the fact that our particles are holes, while $\varepsilon_i(k_H)$ is the i -th energy level for an electron with $k_3 = k_H$ (the result differs by an additive constant corresponding to the valence band fully occupied by electrons).

IV. DETAILS OF THE ALGORITHM

Calculation of G_c according to Eq. (12) requires precise knowledge of the energy levels $\varepsilon_i(k_H)$. In contrast to the case $\gamma_2 = \gamma_3$, the eigenproblem for energy levels does not decompose into 6×6 blocks. Therefore, we have to generate a truncated matrix of the Hamiltonian, and select from its eigenvalues only those that approximate eigenvalues of the infinite matrix. Our Hamiltonian is of the form $\mathcal{H} = h_1 \otimes 1 + h_n \otimes n + h_a \otimes a + h_{a^\dagger} \otimes a^\dagger + h_{a^2} \otimes a^2 + h_{a^{\dagger 2}} \otimes a^{\dagger 2}$, where h_1 , h_n , h_a , and h_{a^2} are 6×6 complex matrices with entries being trigonometric expressions in the angles (θ, ϕ) specifying the direction of the magnetic field.

Instead of just truncating the operators (a, a^\dagger) at some n_{max} , we employ a procedure that is accurate for $\gamma_2 = \gamma_3$ in the sense that the generated matrix of the Hamiltonian is truncated at the non-zero 6×6 -block boundary. This requires applying to \mathcal{H} a unitary transformation $\mathcal{H} \rightarrow \mathcal{R}\mathcal{H}\mathcal{R}^{-1}$, where $\mathcal{R} = \mathcal{R}(\theta, \phi)$ is a 6×6 unitary matrix that implements a rotation from the crystal back to the “1”, “2”, “3” coordinate system, so that in the spherical case the resulting matrix does not depend on (θ, ϕ) . Then, since in the spherical case the wavefunctions assume the form $(c_1 u_n, c_2 u_{n+1}, c_3 u_{n+2}, c_4 u_{n+3}, c_5 u_{n+1}, c_6 u_{n+2})$, where c_i are the unknown components of the eigenvectors, from the transformed $6(n_{max} + 1) \times 6(n_{max} + 1)$ matrix we drop columns and rows numbered $-18, -12, -11, -8, -6, -5, -4, -2, -1$ (the sign minus means counting from the right/bottom), so as to preserve a number of whole 6×6 blocks in which (in the spherical case) the Hamiltonian matrix is non-zero.

The generated matrix is diagonalized using the LAPACK algorithm for band Hermitian matrices (only the eigenvalues are computed)¹⁵. An eigenvalue is then selected as correct if for two subsequent sizes of the truncated matrix we obtain eigenvalues that are the same

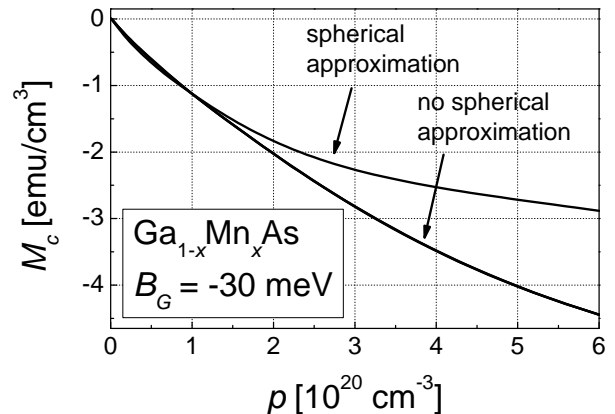


FIG. 1: Hole liquid contribution to volume magnetization, $M_c(p)$ as a function of the hole density p for $\gamma_2 = \gamma_3$ (“spherical approximation”, Refs. 2, 5) and for the real band structure parameters of GaAs (“no spherical approximation”). The spin splitting corresponds to the saturation value of magnetization for Mn concentration $x = 0.05$. The calculations have been carried out for Mn magnetization along three principal crystallographic directions.

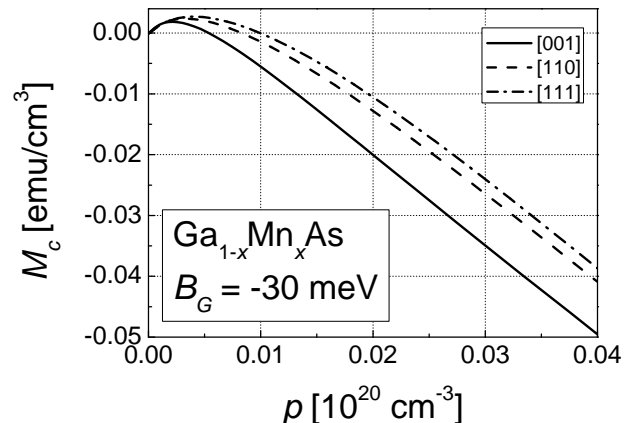


FIG. 2: The curves of Fig. 1 at low hole densities assuming various directions of Mn magnetization.

within the numerical precision (this is called the “second truncation” test in Ref. 8). Great care must be undertaken because the set of selected eigenvalues does not have to be complete unless n_{max} is large enough, *i.e.* there may be some lacking eigenvalues in the range between the smallest and the largest eigenvalues selected. The minimal selected eigenvalue does not monotonically decrease with increasing n_{max} in such a case. That is why we choose $n_{max} \approx 5000$ as a starting point *e.g.* for the [110] direction of the magnetization \mathbf{M} .

V. RESULTS

We have performed computations for (Ga,Mn)As adopting the previously employed values of the band structure parameters and p-d exchange integral.² Figure 1 presents the determined values of the hole magnetization for three principal crystallographic directions of magnetization, compared to the data obtained for the case $\gamma_2 = \gamma_3 = 2.58$, which reproduce the earlier results.^{2,5} The value of the spin splitting parameter $B_G = -30$ meV has been assumed, which corresponds to an effective Mn concentration $x_{\text{eff}} = 0.05$ if magnetization is saturated. As seen, the curves for the three crystallographic directions [001], [110] and [111] of Mn magnetization overlap and are indistinguishable. This demonstrates that a strong warping of the valence band does not result in anisotropy of the hole magnetization in the experimentally important range of the hole concentrations p . A magnified view of the region near $p = 0$ is presented in Fig. 2 to show that in this range a small anisotropy of $M_c = 0$ becomes visible.

The dependence of the carrier magnetization M_c on the Mn magnetization M is presented in Fig. 3. Three curves for different values of the parameter B_G (-10 , -20 , and -30 meV) are displayed. For comparison, the data for $B_G = 10$ meV and $\gamma_2 = \gamma_3 = 2.58$ are also shown. An important aspect of the results depicted in Figs. 1 and 3 is that the approximation $\gamma_2 = \gamma_3 = 2.58$ employed previously underestimates significantly the magnitude of the hole magnetization. An accurate comparison between experimental and theoretical results is, however, somewhat hampered by a relatively large uncertainty in the experimental value of M_c , whose determination from magnetization measurements requires accurate information on the effective Mn concentration. Nevertheless, as an example we consider two samples with $x = 0.05$, *i.e.* $B_G = -30$ meV, and hole concentrations $p = 4.4 \cdot 10^{20}$ and $8.4 \cdot 10^{20}$ cm⁻³. For

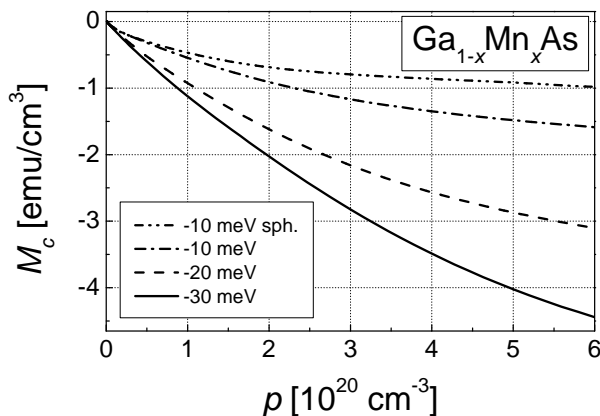


FIG. 3: Hole magnetization $M_c(p)$ for various magnitudes of valence band exchange splitting (B_G equal -10 , -20 , and -30 meV).

Sample No.	1	2	3
Experiment			
n_h -MF [cm ⁻³]	$1.24 \cdot 10^{20}$	$1.48 \cdot 10^{20}$	$1.64 \cdot 10^{20}$
g_{eff}	1.92 ± 0.04	1.87 ± 0.03	1.80 ± 0.02
Theory			
\mathcal{P}	0.836	0.828	0.822
M_c/μ_B [cm ⁻³]	$-1.46 \cdot 10^{20}$	$-1.69 \cdot 10^{20}$	$-1.84 \cdot 10^{20}$
g_{eff}	1.90	1.89	1.88

TABLE II: Comparison of effective Landé factor determined by ferromagnetic resonance (Ref. 6) to theoretical values obtained in the present work.

these samples the previous model predicts $M_c = -0.25$ and $-0.32 \mu_B$ per one Mn ion, respectively. The current theory leads to $M_c = -0.36$ and $-0.49 \mu_B$. These sets of results can be compared to the experimental data, $M_c = -0.36$ and $-0.80 \mu_B$, which we have obtained by taking a mean value of M_c , as measured for $x = 0.045$ and 0.056 before and after annealing.⁵ We see that the present theory describes better the experimental findings but, as mentioned above, more quantitative comparisons requires detail information on the concentration of Mn spins that are not compensated by the antiferromagnetic coupling to interstitial Mn neighbors.

Another relevant experiment is ferromagnetic resonance, which leads to the magnitude of the effective Landé factor systematically smaller than 2, an effect taken as evidence for the hole contribution to the magnetization dynamics.⁶ A comparison of our calculations with the experimental data of Ref. 6 is given in Table II. The theoretical values of g_{eff} have been calculated assuming $n_{\text{Mn}} = 1.01 \cdot 10^{21}$ cm⁻³, $B_G = -30$ meV, and using the formula similar to Eq. 2 of Ref. 6:

$$\frac{Sg_{\text{Mn}}n_{\text{Mn}} + M_c/\mu_B}{g_{\text{eff}}} = Sn_{\text{Mn}} + sn_h\mathcal{P}, \quad (13)$$

where $S = 5/2$, $g_{\text{Mn}} = 2.0$, $s = 1/2$, and \mathcal{P} is the hole liquid spin polarization defined in Eq. 11 of Ref. 2. We see that our theory describe satisfactorily the deviation of the value of the effective Landé factor from 2, although for the sample with the highest T_C the deficit of the magnetization is still larger than our calculation predicts. This disagreement may result from an underestimation of the experimental value of the hole concentration that was *calculated* based on the value of T_C .⁶

VI. CONCLUSIONS

In our work, presumably for the first time, an efficient approach has been proposed allowing for the calculation of the Landau level energies in the valence band within the $\mathbf{k} \cdot \mathbf{p}$ model of zinc-blende materials for an arbitrary direction of the magnetic field and non-zero hole momentum k_H taking effects of cubic anisotropy into account.

The model has been employed to evaluate the contribution of kinetic and spin energies to the volume magnetization of the holes in (Ga,Mn)As. Surprisingly, the evaluated crystalline anisotropy of the carrier magnetization in the relevant range of the hole densities is negligibly small. At the same time we have found that the magnitude of M_c is about 50% larger than that calculated earlier in the spherical approximation. We have demonstrated that our improved theory describes better the available results of magnetization measurements⁵ and magnetic resonance⁶ studies.

Acknowledgments

This work was supported in part by ERATO Semiconductor Spintronics Project of Japan Science and Technology Agency and NANOSPIN E. C. project (FP6-2002-IST-015728). The computations has been in part performed at the Interdisciplinary Centre for Mathematical and Computational Modelling, Pawinskiego 5A, PL-02-106, Warsaw.

* Electronic address: sliwa@ifpan.edu.pl

† Electronic address: dietl@ifpan.edu.pl

¹ T. Dietl, H. Ohno, *Ferromagnetic III-V and II-VI Semiconductors*, MRS Bulletin, October 2003, p. 714.

² T. Dietl, H. Ohno, F. Matsukura, Phys. Rev. B **63**, 195205 (2001).

³ T. Jungwirth, Jairo Sinova, J. Mašek, J. Kučera, A. H. MacDonald, Rev. Mod. Phys. **78**, 809 (2006); arXiv:cond-mat/0603380; <http://unix12.fzu.cz/ms/>.

⁴ T. Dietl, H. Ohno, F. Matsukura, J. Cibert, D. Ferrand, Science **287**, 1019 (2000).

⁵ T. Jungwirth, J. Masek, K. Y. Wang, K. W. Edmonds, M. Sawicki, M. Polini, J. Sinova, A. H. MacDonald, R. P. Campion, L. X. Zhao, N. R. S. Farley, T. K. Johal, G. van der Laan, C. T. Foxon, B. L. Gallagher, Phys. Rev. B **73**, 165205 (2006); arXiv:cond-mat/0508255.

⁶ X. Liu, W. L. Lim, M. Dobrowolska, J. K. Furdyna, T. Wojtowicz, Phys. Rev. B **71**, 035307 (2005).

⁷ J. M. Luttinger, Phys. Rev. **102**, 1030 (1955).

⁸ R. L. Bell, K. T. Rogers, Phys. Rev. **152**, 746 (1966).

⁹ C. R. Pidgeon, R. N. Brown, Phys. Rev. **146**, 575 (1966).

¹⁰ H.-R. Trebin, U. Rössler, R. Ranvaud, Phys. Rev. B **20**, 686 (1979).

¹¹ P. Pfeffer, W. Zawadzki, Phys. Rev. B **41**, 1561 (1990); P. Pfeffer, W. Zawadzki, Phys. Rev. B **53**, 12813 (1996).

¹² L. D. Landau, E. M. Lifshitz, *Quantum Mechanics* (Pergamon Press, London, Paris, 1958).

¹³ B. Lang, SIAM J. Sci. Comput. **14**, 1320 (1993).

¹⁴ Our basis is related to that of Ref. 2 Appendix A as follows: $u_1 = -|\frac{3}{2}, \frac{3}{2}\rangle$, $u_2 = -i|\frac{3}{2}, \frac{1}{2}\rangle$, $u_3 = |\frac{3}{2}, -\frac{1}{2}\rangle$, $u_4 = i|\frac{3}{2}, -\frac{3}{2}\rangle$, $u_5 = |\frac{1}{2}, \frac{1}{2}\rangle$, $u_6 = -i|\frac{1}{2}, -\frac{1}{2}\rangle$.

¹⁵ See Ref. 13 for an alternative, parallelizable, algorithm that has been implemented for real symmetric matrices and probably can be generalized to complex Hermitian matrices.